GENERALIZABLE COARSE-TO-FINE ROBOT MANIPU-LATION VIA LANGUAGE-ALIGNED 3D KEYPOINTS

Anonymous authors

Paper under double-blind review

ABSTRACT

Hierarchical coarse-to-fine policy, where a coarse branch predicts a region of interest to guide a fine-grained action predictor, has demonstrated significant potential in robotic 3D manipulation tasks by especially enhancing sample efficiency and enabling more precise manipulation. However, even augmented with pre-trained models, these hierarchical policies still suffer from generalization issues. To enhance generalization to novel instructions and environment variations, we propose Coarse-to-fine Language-Aligned manipulation Policy (CLAP), a framework that integrates three key components: 1) task decomposition, 2) VLM fine-tuning for 3D keypoint prediction, and 3) 3D-aware representation. Through comprehensive experiments in simulation and on a real robot, we demonstrate its superior generalization capability. Specifically, on GemBench, a benchmark designed for evaluating generalization, our approach achieves a 12% higher average success rate than the SOTA method while using only 1/5 of the training trajectories. In real-world experiments, our policy, trained on only 10 demonstrations, successfully generalizes to novel instructions and environments.

1 Introduction

Robot learning, especially via imitation learning, has demonstrated promising success in enabling robots to solve complex 3D manipulation tasks (Intelligence et al., 2025; Liu et al., 2024). However, scaling these methods to a broader range of real-world applications (e.g., industrial, service, or home robotics) requires enhancing both (G1) their generalization to environment variations, and (G2) their skill compositional generalization. Indeed, G1 is necessary, because deployed robots need to be able to operate in new settings (e.g., object or background variation), while G2 is highly desirable, so that trained robots can tackled new tasks by composing previously-learned skills. To achieve G1 and G2, the robot needs to be endowed with a combination of capabilities, such as scene understanding, reasoning or planning, and high-precision manipulation, exploiting preferably sample efficient techniques, since robotics data is costly to collect.

In this paper, we focus on one type of 3D manipulation policies, called coarse-to-fine policies (Gualtieri & Platt, 2020; James et al., 2022; Ling et al., 2024; Goyal et al., 2024; Gervet et al., 2023; Liu et al., 2025), because they achieve superior precision in manipulation tasks while enjoying strong sample efficiency. These policies process 3D observations (or 3D scene representations) using a hierarchical architecture whose higher-level coarse branch identifies a region of interest for the lower-level fine-grained branch to focus on and predict a final action. Typically, the coarse branch is trained to predict a 3D keypoint, which serves as the center for cropping and zooming into the original 3D observations. To help with visual understanding and to some extent spatial reasoning, recent work (Li et al., 2025b; Fang et al., 2025) has extended this approach to exploit pre-trained models—Vision-Language Models (VLMs) (Beyer et al., 2024) or visual foundation models (Ravi et al., 2024). However, the performance of these obtained methods is still limited in terms of generalization capability (G1 and especially G2), indicating that their scene understanding and reasoning capabilities are actually still rudimentary. Our experimental study suggests that this is primarily due to a combination of various issues (depending on the method), such as domain shift between pre-training and robotic images, inadequacy of pre-trained models to predict 3D keypoint, poor adaptation to object variations, or under-exploitation of the planning ability of VLMs.

Figure 1: **Intuition of CLAP.** Our method achieves strong generalization ability by decomposing tasks into step-wise language instructions, each aligned with a 3D keypoint.

To address these limitations and issues, we propose Coarse-to-fine Language-Aligned manipulation Policy (**CLAP**), a novel coarse-to-fine 3D manipulation policy. In contrast to previous coarse-to-fine policies, CLAP includes a novel architecture for the higher-level branch, which we name *coarse task planner*, and a novel implementation of the lower-level fine-grained action predictor, both leveraging pre-trained models.

The coarse task planner, implemented as a VLM, is introduced to play the additional role of task planning. Before the usual 3D keypoint prediction, it decomposes a task into step-wise language instructions, representing basic skills. This change allows both 3D keypoint and action predictions to depend on step-wise instructions instead of the whole task description, which promotes skill compositional generalization (G2). The training of this coarse task planner consists of three parts to reinforce its scene understanding and reasoning capabilities. First, the pre-trained VLM fine-tuned on language plans of different tasks to directly improve compositional reasoning. Second, it is specialized for 3D keypoint prediction by fine-tuning it to perform a sequential reasoning process: first localizing task-related objects, then generating the step instruction, and finally predicting a corresponding 3D keypoint. Finally, to further boost its scene understanding capability, the VLM is further fine-tuned with an auxiliary task of 3D object detection, using an additional dataset of object positions. Together, these components form a comprehensive pipeline that significantly enhances the generalization ability of the coarse-to-fine policy to object variations (G1) and novel tasks (G2).

The fine-grained action predictor takes as input both the step instruction and the multi-view RGB-D images and outputs an action. It is implemented with specialized pre-trained models to improve sample efficiency and increase its precision during manipulation. More specifically, step instruction and RGB images are processed using a pre-trained visual-language encoder, ensuring the two modalities are well-aligned. The depth information is processed by a dedicated encoder and augmented with 3D position embeddings to help better align 3D and 2D image information. All the obtained embeddings, which we call 3D-aware representation, are fused via a Multi-View Transformer (Goyal et al., 2023) to predict the final actions.

To evaluate the performance of our method, we run experiments in both simulation and real-world. For simulation, we use GemBench (Garcia et al., 2025), a benchmark specifically designed to assess the generalization ability of multi-task language-conditioned policies across varying difficulty levels. Our approach outperforms the state-of-the-art method, achieving a 12% higher average success rate with only 1/5 of the training trajectories. In real-world experiments, our method demonstrate strong generalization ability to novel tasks and object variations with only 10 demonstrations per task.

Contributions

- 1. We introduce a novel coarse-to-fine 3D manipulation policy, as shown in Figure 1, with two main innovations: (1) tasks are decomposed into step-wise language instructions to promote compositional generalization ability; (2) action inference is performed via a reasoning step to improve generalization to object variations.
- 2. We design a finetuning pipeline that effectively adapts a pre-trained VLM to 3D keypoint prediction and incorporate a 3D-aware representation in the fine-grained action predictor, overcoming the issues observed in previous methods.
- 3. Empirical evaluations in simulation and on a real robot demonstrate state-of-the-art performance in both robustness to visual and object changes and generalization to unseen tasks.

2 RELATED WORK

108

109 110

111

112113114

115

116

117

118

119

120

121

122

123

124

125

126

127

128

129

130

131

132

133 134 135

136

137

138

139

140

141

142

143

144

145

146 147

148

149

150

151

152

153

154

155

156

157

158

159

160

161

In this section, we discuss the related works in the field, including vision-language-action models, 3D manipulation policies, and coarse-to-fine policies.

Vision-Language-Action (VLA) models Training VLMs (OpenAI, 2024; Beyer et al., 2024; Bai et al., 2025; AI, 2024) on vast internet-scale image-text corpora has led to remarkable capabilities in image understanding, excelling at tasks like image classification, object detection, and visual question answering tasks. However, applying a similar training strategy directly to robotics presents a challenge due to the relatively scarce robot trajectory data. A prominent solution is to transfer the knowledge from pre-trained VLMs by fine-tuning them on robot data. This approach is the foundation for recent VLA models (Driess et al., 2023; Brohan et al., 2023; Kim et al., 2024; Octo Model Team et al., 2024; Intelligence et al., 2025; Wen et al., 2025a; Shukor et al., 2025; Liu et al., 2024; Wen et al., 2025b; Li et al., 2024; Cheang et al., 2025; Team et al., 2025; NVIDIA et al., 2025), which are fine-tuned on large diverse datasets of robot trajectories. Such extensive training strengthens generalization to novel objects, environments, and tasks. However, since they commonly use multi-view 2D images as visual input, learning to reason in 3D space from 2D images alone is data-intensive. This leads to sample inefficiency and low success rates on some tasks. Recent work has sought to more explicitly incorporate 3D information (Li et al., 2025a; Qu et al., 2025; Zhen et al., 2024) or introduce Chain of Thought (Mu et al., 2023; Zawalski et al., 2024; Zhao et al., 2025) to enhance the 3D reasoning ability. However these directions remain relatively underexplored within the VLA paradigm. Our method, which fine-tunes a pretrained VLM as a coarse task planner and predicts the final action with a fine-grained action predictor, can also be viewed as a VLA model. In contrast to other VLA approaches, we propose specific training and inference techniques to better align pre-trained VLMs to 3D manipulation, further enhancing generalization (G1-G2) while retaining the sample efficiency inherent to hierarchical coarse-to-fine policies.

3D Manipulation Policy 3D manipulation policies (Shridhar et al., 2022; Gervet et al., 2023; Jia et al., 2025; Zhu et al., 2025; Wang et al., 2024b; Ze et al., 2024; Wang et al., 2024a; Goyal et al., 2024; Ke et al., 2024; Fang et al., 2025; Li et al., 2025b; Garcia et al., 2025) directly work with 3D inputs and outputs. They generally include structured architectures that construct a 3D representation of the scene, leading to higher sample efficiency and better generalization to new camera viewpoints. For example, PerAct (Shridhar et al., 2022) explicitly represents the scene with a voxel representation. Gervet et al. (2023) and Ke et al. (2024) process RGB images with pre-trained image encoder and lift 2D features to 3D by aggregating with depth information. An alternative approach (Jia et al., 2025; Goyal et al., 2024) is to project point clouds into canonical virtual views and use the resulting multi-view images as input. Explicitly exploiting 3D information allows these models to achieve high success rates with much less training data, which can be further reduced by enforcing a hierarchical structure like in coarse-to-fine policies.

Coarse-to-fine Policies Gualtieri & Platt (2018; 2020) first propose this coarse-to-fine scheme for pick-and-place tasks. Subsequent work has considered more general tasks and explored various 3D representations, such as voxel observations (James et al., 2022; Liu et al., 2025), 3D feature fields (Gervet et al., 2023), and multi-view images (Goyal et al., 2024). Ling et al. (2024) apply the coarse-to-fine architecture to handle noisy point clouds. Among these, Robotic View Transformer 2 (RVT2) (Goyal et al., 2024) is an effective language-conditioned multi-task policy, demonstrating strong performance in both training and inference efficiency by using multi-view images projected from canonical views. However, RVT2 is trained from scratch, which limits its generalization ability to visual perturbations and task variations. Subsequent efforts built upon this work have sought to overcome these limitations. Existing works (Li et al., 2025b; Fang et al., 2025) have attempted to enhance generalization through strategies such as: pre-training on object detection datasets (Yuan et al., 2024) or integrating encoders from powerful visual foundation models like Segment Anything Model 2 (Ravi et al., 2024). In contrast, we achieve this by introducing a novel architecture, where tasks are decomposed into step-wise language instructions for skill compositional generalization and design a specific training and inference pipeline to leverage pre-trained models in both coarse and fine-grained branches.

3 BACKGROUND

In this section, we first briefly recall the multi-task imitation learning set-up, introduce coarse-to-fine policy, and then present Robotic-View-Transformer 2 (RVT2) (Goyal et al., 2024), a state-of-the-art coarse-to-fine policy that serves as the foundation for our method.

In multi-task imitation learning, a dataset $\mathcal{D} = \{(\tau_i, L_i) \mid i = 1, ..., N\}$ is available for pairs of robot demonstrations τ_i and task description L_i . Index i may be dropped if not needed. A robot demonstration is a trajectory $\tau_i = (o_0, a_0, o_1, a_1, ...)$ containing a sequence of observations o_t and corresponding expert actions a_t . Observations include multi-view RGB-D images and gripper status indicating whether it is close or open. Actions denote the state of the end-effector, which contains the 3D position $p_t = (x_t, y_t, z_t)$ of the gripper, the orientation of the gripper and a gripper status.

A coarse-to-fine policy contains a coarse branch and a fine-grained branch, where the coarse branch predicts a 3D keypoint as the center to zoom in the 3D observation and the fine-grained branch uses the refined observation to predict the target action. Such policy is trained according to the key-frame based imitation learning framework (Johns, 2021; Shridhar et al., 2022; Goyal et al., 2024). Specifically, key-frames identifies timesteps in a trajectory when an important action, like grasping or placing, occurs. In practice, they are usually heuristically defined for each trajectory. With these key-frames, a trajectory is segmented into K subsequences of observations and actions $(o_0, a_0, ..., o_{t_1}, a_{t_1}), ..., (o_{t_{K-1}+1}, a_{t_{K-1}+1}, ..., o_{t_K}, a_{t_K})$, where the k^{th} key-frame occurs at time step t_k , from which we can extract a sequence of key-frame actions $(a_{t_1}, ..., a_{t_K})$. In this framework, the goal is to train a policy π to predict the key-frame action a_{t_k} at the closest next key-frame of timestep t_k given an observation o_t and a task description L_i :

$$\pi(o_t, L_i) \to a_{t_k} \text{ for } t_{k-1} \le t < t_k. \tag{1}$$

The predicted actions are executed by a motion planner, which moves the robot to the desired state, generating thus the intermediate actions in a trajectories. In coarse-to-fine policies, the 3D position p_{t_k} output by the coarse branch for the next key-frame is typically used as the 3D keypoint to zoom into the observation for the action predictor.

In RVT2, multi-view RGB-D images are first aggregated into a point cloud, which is then projected into three canonical views: front, left and top. These three views are orthogonal to each other, which allows a mapping between pixel positions in these views and a 3D position in the scene. Each pixel in the projected images contains 3-channel RGB values, 1-channel depth value and its corresponding 3D position in the global coordinate. In the coarse branch, the projected images are tokenized using convolutional layers while the task description and robot states (e.g., gripper status) are encoded by a pre-trained language encoder and a trainable Multi-Layer-Perceptron respectively. All these tokenized features are fused via Multi-View Transformer (Goyal et al., 2023). The image tokens in the output of the transformer are then processed by upsampling layers to predict heatmaps, from which a 3D keypoint is extracted. The keypoint from the coarse branch is used to zoom in and crop the point cloud while the cropped region is again projected into the canonical views. The refined observations along with the same task description are processed by the fine-grained branch, implemented as another multi-view transformer with different weights, to predict the final actions. While RVT2 achieves strong sample efficiency and enables precise manipulation via projections to canonical views and its coarse-to-fine architecture, it is trained from scratch and therefore does not leverage recent pretrained large models. In addition, its architecture design does not fully exploit common skills among tasks. As a result, it suffers from deficient generalization to visual changes, object variations, and novel tasks.

4 METHOD

Our hierarchical policy consists of a coarse task planner and a fine-grained action predictor, as shown in Figure 2. To promote compositional generalization, we first decompose tasks into step-wise language instructions, each describing the motion of the robot between two consecutive key-frames. This enables the coarse task planner to perform language-guided planning while allowing the fine-grained action predictor to learn and reuse common skills across tasks. Moreover, we adapt a pre-trained VLM to 3D keypoint prediction in the coarse task planner, by finetuning it with a sequential reasoning procedure. The pretrained VLM is trained to first reason about the positions

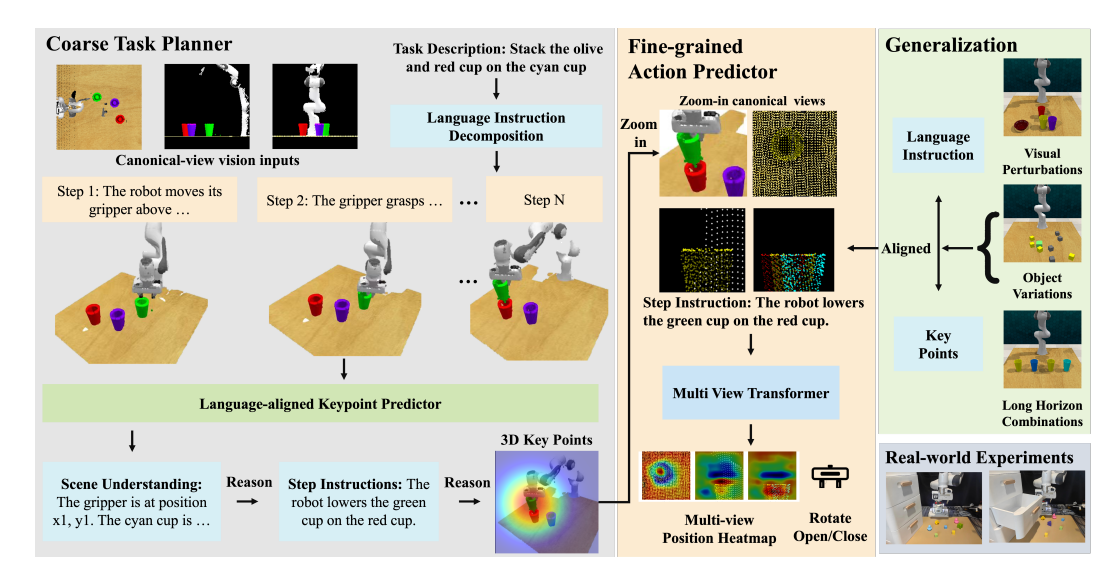


Figure 2: **Overview of CLAP.** We propose a novel coarse-to-fine 3D manipulation policy, comprising of a coarse task planner and a fine-grained action predictor. The coarse task planner reasons about the task plans and the positions of task-related objects to generate language-aligned 3D keypoints. The fine-grained action predictor fuses the corresponding step instruction with a 3D-aware visual representation from refined observations to predict the final action.

of task-related objects, then generate a step instruction and finally predict the corresponding 3D keypoints. To enable zero-shot generalization ability to novel objects, we add an auxiliary task of 3D object detection by augmenting the training data with additional object positions dataset. Finally, in contrast to RVT2, the coarse and fined-grained branches are implemented with a different architecture, since they play different roles. Thus, for the latter, we utilize specialized pre-trained visual foundation models to construct a 3D-aware representation. The design choices of both the coarse task planner and the fine-grained action predictor are detailed in the following sections.

4.1 COARSE TASK PLANNER

Prior coarse-to-fine policies condition all actions within a trajectory on a single high-level task description, limiting compositional generalization. To address this, we leverage a pre-trained VLM, denoted f_{θ} , to decompose a high-level task description L into step-wise language instructions $\mathcal{L} = (\ell_1, ..., \ell_k, ..., \ell_K)$, which naturally align with the key-frame based trajectory segmentation. Each trajectory segment $(o_{t_{k-1}+1}, a_{t_{k-1}+1}, ..., o_{t_k}, a_{t_k})$ and key-frame action a_{t_k} have a corresponding step instruction ℓ_k describing the motion of the robot within the segment. For example, the task "open the top drawer" is decomposed into following step instructions: ℓ_1 : "The robot arm lowers itself to align with the handle of the top drawer", ℓ_2 : "The robot arm grasps the top drawer's handle firmly", and ℓ_3 : "The robot pulls the handle back, smoothly opening the top drawer".

In addition to task decomposition done at the beginning, at every execution timestep, the VLM f_{θ} is also exploited to predict both the step instruction ℓ_{t_k} (used as a novel input of the action predictor) and its language-aligned 3D keypoint p_{t_k} (for cropping a region of interest, as usually done in coarse-to-fine policies). We discuss next how this prediction can be realized effectively.

Task decomposition enables reasoning about task plans before predicting actions. However, directly training the model f_{θ} to simultaneously generate a task plan \mathcal{L} and predict step instruction ℓ_{t_k} and 3D keypoint p_{t_k} , given as inputs multi-view images obtained from observation $o_{t_{k-1}}$ and a high-level task description L, (i.e., $f_{\theta}(o_{t_{k-1}}, L) \to (\mathcal{L}, \ell_{t_k}, p_{t_k})$), does not ensure generalization to novel instructions. Previous studies (Kim et al., 2024; Intelligence et al., 2025; Zhao et al., 2025; Gao et al., 2025) indicate that VLAs exhibit a strong bias towards visual inputs, due to the richer information embedded in the visual inputs. This reliance often causes failures to follow novel language instructions. Under our data-scarce training setting, this issue is intensified by the limited diversity of language instructions. To address this issue, we propose decoupling task planning from

keypoint prediction via a two-round inference protocol. First, a purely textual query generates a language plan, the sequence of all step instructions \mathcal{L} . Second, the visual inputs augmented with this plan are used to predict the corresponding step instruction and keypoint:

$$f_{\theta}(L_i) \to \mathcal{L}, f_{\theta}(o_{t_{k-1}}, \mathcal{L}) \to (\ell_{t_k}, p_{t_k}).$$
 (2)

This approach not only mitigates visual bias but also enables training with an auxiliary dataset of language plans, which serves as a manual to enhance compositional task reasoning.

For a plan \mathcal{L} corresponding to a task description L, directly fine-tuning a VLM to predict both the step instruction ℓ_{t_k} and its language-aligned 3D keypoint p_{t_k} reveals to be insufficient due to the inadequate alignment of the visual-textual embeddings of the VLM for this 3D keypoint prediction. Instead, inspired by Chain-of-Thought reasoning (Mu et al., 2023; Zawalski et al., 2024; Zhao et al., 2025) for robotics, we design a reasoning process by training our model to first reason about the pixel positions of task-related objects, then generate a step instruction and finally predict the corresponding keypoint, changing the second step of Equation (2) to:

$$f_{\theta}(o_{t_{k-1}}, \mathcal{L}) \to (\boldsymbol{p}_{obj}, \ell_{t_k}, p_{t_k}),$$
 (3)

where p_{obj} are the 3D positions of the task-related objects.

We further observe that for long-horizon, especially repetitive tasks (e.g., "stack several blocks"), only providing the entire task plan whether as input or output can degrade the performance. This often causes the model to generate repetitive sequences until reaching the output length limit or to struggle in determining the next step from an excessively long plan. To mitigate this, we introduce two ideas. First, we provide to the VLM an additional input: the step instruction predicted in the last timestep, which serves as a short-term memory cue to contextualize the current situation. Moreover, we decompose the plan into sub-tasks, i.e., $\mathcal{L} = \left(\mathcal{L}_1 = (\ell_1, \ell_2, ..., \ell_n), \mathcal{L}_2 = (\ell_{n+1}, \ell_{n+2}, ...), ...\right)$.

For instance, "stack the blue and yellow cup on the red cup" is decomposed into two sequential sub-tasks: \mathcal{L}_1 "stack the blue on the red cup" followed by \mathcal{L}_2 "stack the yellow cup on the red cup". The model is trained to generate only the task plan of current sub-task, preventing repetition and improving focus:

$$f_{\theta}(L,\hat{\ell}) \to \mathcal{L}_m, f_{\theta}(o_{t_{k-1}}, \mathcal{L}_m, \hat{\ell}) \to (p_{obj}, \ell_{t_k}, p_{t_k}),$$
 (4)

where $\hat{\ell}$ is the step instruction predicted in the last timestep and \mathcal{L}_m is the language plan of the m^{th} sub-task. At the beginning of a trajectory, where no previous timestep exists, $\hat{\ell}$ is defined as "the robot is currently at the initial state" to indicate the initial state.

To further enhance the generalization ability of the coarse task planner to object variations, we include an auxiliary task of predicting the object positions. We randomly initialize diverse environments and record the RGB-D images of the scene along with the 3D positions of the objects. Following the same pre-processing, both the RGB-D images and the 3D positions of the objects are projected into canonical views. The projected multi-view images and pixel coordinates of the object positions in each view are used to construct an object position dataset. This dataset is then utilized to co-train the VLM, reinforcing its spatial understanding and improving zero-shot generalization to object variations.

4.2 Fine-grained Action Predictor

The fine-grained action predictor uses a predicted step instruction ℓ_{t_k} , instead of the original high-level task description L, enabling more precise and generalizable skill learning. Considering the significant domain shift between the images focused around predicted p_{t_k} from those used to pretrain standard VLMs, we decide to employ instead pre-trained specialized encoders to process these inputs. Our feature encoding pipeline consists of three stages to construct a unified 3D-aware and language-aligned representation. First, RGB images and step instructions are processed through vision-language encoders to establish semantic alignment between visual and textual inputs. Second, depth images are encoded separately to extract explicit geometric structure. Finally, we generate a 3D position embedding from pixel-wise 3D coordinates to incorporate spatial awareness. These components are combined to form a 3D-aware, language-aligned representation for downstream fine-grained action prediction, following the architecture of prior work (Goyal et al., 2024).

Models	Avg. Success ↑	L1	L2	L3	L4
HiveFormer (Guhur et al., 2023)	30.4	60.3 ± 1.5	26.1 ± 1.4	35.1 ± 1.7	0.0 ± 0.0
PolarNet (Chen et al., 2023)	38.4	77.7 ± 0.9	37.1 ± 1.4	38.5 ± 1.7	0.1 ± 0.2
3D Diffuser Actor (Ke et al., 2024)	44.0	91.9 ± 0.8	43.4 ± 2.8	37.0 ± 2.2	0.0 ± 0.0
RVT2 (Goyal et al., 2024)	44.0	89.1 ± 0.8	51.0 ± 2.3	36.0 ± 2.2	0.0 ± 0.0
3D-LOTUS (Garcia et al., 2025)	45.7	94.3 ± 1.4	49.9 ± 2.2	38.1 ± 1.1	0.3 ± 0.3
3D-LOTUS++ (Garcia et al., 2025)	48.0	68.7 ± 0.6	64.5 ± 0.9	41.5 ± 1.8	17.4 ± 0.4
BridgeVLA (Li et al., 2025b)	50.0	91.1 ± 1.1	65.0 ± 1.3	43.8 ± 1.2	0.0 ± 0.0
CLAP (Proposed)	62.0	83.9 ± 0.3	83.2 ± 1.9	49.6 ± 2.1	$\textbf{31.4} \pm 0.6$

Table 1: **Multi-Task Performance on GemBench.** Here are the average success rates of 4 levels of evaluation tasks from Gembench. Except CLAP, we use the results reported in BridgeVLA.

5 EXPERIMENTS

We now present the experimental settings and results in simulation and real-world experiments.

5.1 SIMULATION RESULTS

Experimental Set-up Our method is evaluated on GemBench (Garcia et al., 2025), a benchmark specifically designed for evaluating the generalization ability of a policy. A dataset containing 100 demonstrations per task along with a task description per trajectory is prepared for training. This training set contains 16 tasks with 31 variations. Within a trajectory, 4 cameras are placed at the front, left shoulder, right shoulder and wrist to collect RGB-D images as the observations. The resolution of the original RGB-D images is 256x256 while the resolution of the projected images is 224x224. Instead of evaluating on in-distribution tasks and variations, GemBench designs an evaluation set containing 4 levels of tasks, where different elements are varied:

- Placements (L1: same 16 tasks (31 variations) as in training set, but with novel object placements.
- Rigid Objects (L2): 15 novel tasks (28 variations) with newly-colored or -shaped rigid objects.
- Articulated Objects (L3): 18 novel tasks (21 variations) with appearance or object variation.
- Long-horizon Tasks (L4): 6 novel long-horizon tasks (12 variations).

The specific configuration for tasks used for training and evaluation in GemBench are listed in Appendix A.1. Following the evaluation setting in GemBench (Garcia et al., 2025), all trained models are evaluated with 20 episodes per task variation per seed, and 5 different seeds are used.

In our method, we finetune Qwen 2.5 VL-3B (Bai et al., 2025) as the coarse task planner. It is LoRA fine-tuned (Hu et al., 2022) with the object keypoint dataset, language plans, and robot trajectories. We use SigLIP (Zhai et al., 2023) to extract features from the RGB images and step instructions, leveraging its language-aligned representations. For depth images, we use DINOv2 (Oquab et al., 2023), which excels at capturing geometric structures like edges and contours. We further enhance these features by using the 3D coordinate of each pixel to construct a 3D position embedding. The hyperparameters, such as batch size and learning rate used in training are listed in Appendix A.2.

To construct the fine-tuning dataset from robot trajectories, we design a sampling strategy to choose samples from the trajectories. Apart from key-frame pairs of observation and action $(o_{t_k}, a_{t_{k+1}})$, RVT2 augments the training data by sampling observations every n frames (e.g., every 10 frames). However, this results in an uneven number of samples per trajectory segment, due to the varying length of each segment. We initially attempted to sample observations within a window $(o_{t_k-m},...,o_{t_k},...o_{t_k+m})$ around the time step t_k of the k^{th} key-frame. However, observations at time steps before a key-frame and after a key-frame are visually similar while corresponding to distinct actions. For example, o_{t_k-1} and o_{t_k+1} are similar while their corresponding keypoints are the gripper positions at t_k and t_{k+1} respectively. Using all observations around the key-frames to fine-tune the VLM risks confusing it. Finally, we choose to use observations $(o_{t_k},...o_{t_k+m})$ at the time steps immediately following each key-frame. We empirically choose m as 5 in all experiments.

Main Results The evaluation results on GemBench are summarized in Table 1, reporting the average success rate for tasks at each generalization level. The detailed success rate for each task are recorded in Appendix A.3. The experimental results demonstrate the strong generalization ability

Exp	Language Plan	Object Keypoints	Last	Reason	Reason	Pretrained	Level	Level	Level	Level	Avg.
ID	Data	Data	Step	Plan	Objects	Encoder	1	2	3	4	Succ.
1	×	X	X	X	X	✓	86.9	68.2	36.4	0.4	48.0
2	X	X	X	X	✓	✓	81.8	74.8	39.0	0	48.9
3	✓	X	X	✓	X	✓	83.4	66.1	41.9	2.0	48.3
4	✓	X	√	✓	√	√	84.8	81.4	43.8	30.4	60.1
5	✓	✓	✓	✓	✓	×	82.4	79.1	44.5	25	57.8
6	✓	✓	√	✓	✓	✓	83.8	83.2	49.6	31.4	62.0

Table 2: **Ablation study of CLAP on GemBench.** Here are the average success rates of 4 levels of evaluation tasks from Gembench under different training settings.

of our method to novel tasks and object variations, as indicated by the performance gain on Level-2, Level-3, and Level-4 tasks. Our method achieves an overall success rate 12% higher than prior state-of-the-art method (Li et al., 2025b). Notably, this improvement is obtained using only 20 trajectories per task variation for training, significantly fewer than the 100 trajectories used by other baselines. Furthermore, our design leads to substantial performance gain on the most challenging Level-4 tasks, where several baselines methods fail consistently.

Ablation We further experimentally validate the design choice for both coarse task planner and fine-grained action predictor on GemBench. The configurations are detailed below and corresponding results are presented in Table 2.

- 1) **Base** In the base version (corresponding to Exp ID 1), the coarse task planner is trained with only the robot trajectories to predict step instruction and the corresponding keypoints. We use this version as a baseline to ablate our method.
- 2) **Object Reasoning** To adapt the pre-trained VLM for 3D keypoint prediction, we introduce a structured reasoning procedure where the model first localizes task-relevant objects before predicting the step instruction and its corresponding keypoint. We evaluate the efficacy of this object position reasoning in Exp ID 2. A comparison with the base model (Exp ID 1) reveals a performance improvement on Level-2 and Level-3 tasks, indicating enhanced generalization to object variations.
- 3) Language Plan Reasoning The proposed task decomposition enables a two-round conversation, where a language plan is first generated through textual reasoning, followed by keypoint prediction. This approach also permits the inclusion of additional language plans during training to enhance compositional generalization. Compared to the base model (Exp ID 1), this version shows improvements on Level 3 and Level 4 tasks, demonstrating stronger generalization to novel task variations.
- 4) **Include Previous Step Instruction** Previous step instruction is included in the input as a short-term memory to help contextualize the current status. This design yields performance gains across Levels 2, 3, and 4, with particularly notable improvements on long-horizon tasks in Level 4.
- 5) **CLAP w/o Pre-trained Encoder** An ablation study (comparing Exp ID 5 and Exp ID 6) on the coarse planner confirms that incorporating the 3D-aware representation contributes to performance gains at all generalization levels.
- 6) **CLAP** Our method integrates all components mentioned above. A comparison between Exp ID 4 and ours can further validate the performance gain from adding the object position dataset.

5.2 REAL-WORLD EXPERIMENTS

Experimental Setting We keep the training settings the same as in the simulation and list key modifications here. In the real-world experiments, we use a single camera (Intel RealSense D435i) to collect RGB-D images of size 640x360. 10 trajectories are collected per task to cover all variations of each task. The hyperparameters used for training the models are listed in Appendix A.2. The training tasks, illustrated in Figure 3, are listed below. 1) Place shape in shape sorter: insert objects into a box with 3 variations on the object shape. 2) Put block in cup: put a colored block in a same-colored cup with 3 variations on colors. 3) Open drawer: open a drawer with 3 variations on the handles. 4) Put a block in drawer: put a colored block in an open drawer with 3 variations on colors.

We assess the generalization ability of CLAP along two key dimensions (see Appendix A.4 for an overview of these evaluation tasks):

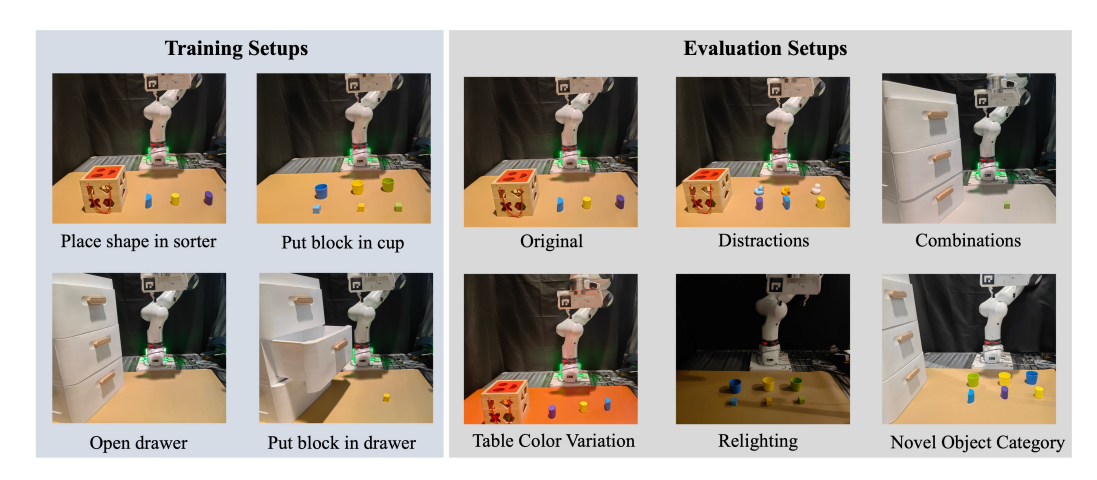


Figure 3: Overview of the tasks in real-world experiments. There are four training tasks: put shape in shape sorter, put block in cup, open drawer, put block in drawer. We evaluate the same tasks under different visual perturbations and novel tasks designed based on the training tasks.

	No Variation		Table Color		Distracted Objects		Light Strength		Average Succ	
	RVT2	CLAP	RVT2	CLAP	RVT2	CLAP	RVT2	CLAP	RVT2	CLAP
place shape in shape sorter	60%	60%	35%	50%	30%	40%	20%	50%	36.2%	50%
put block in cup with same color	40%	100%	20%	70%	20%	80%	20%	80%	25%	82.5%
open drawer	100%	100%	85%	95%	100%	100%	0%	100%	71.2%	98.7%
put block in open drawer	40%	90%	25%	90%	20%	70%	0%	90%	21.2%	85%
put block in cup with different color	20%	100%	15%	70%	0%	70%	10%	80%	11.2%	80%
put shape in open drawer	30%	80%	20%	65%	10%	70%	0%	80%	15%	73.7%
put shape in cup	0%	80%	0%	70%	0%	60%	0%	70%	0%	70%
put block in close drawer	0%	90%	0%	75%	0%	70%	0%	80%	0%	78.7%
average success rate	36.2%	87.5%	25%	73.1%	22.5%	70%	6.2%	78.7%	22.5%	77.3%

Table 3: **Real-world Performance.** Here are the average success rate under different generalization settings for real-world experiments.

- 1) **Visual Perturbations**: The model is tested on the tasks same as the training tasks but with the following conditions: different table colors, introducing distracting objects and altered backgrounds.
- 2) **Task/Object Variations**: Generalization is evaluated through: i) Object substitution (e.g., placing a "shape" object into a cup), and ii) Skill composition (e.g., combining "open drawer" and "place block" into a single, sequential task).

Results The results of evaluating the trained models in real-world experiments are summarized in Table 3. Our method achieves a strong generalization ability to novel tasks and object variations, trained with only 10 demonstrations per task. CLAP achieves 54.8% higher average success rates compared to RVT2 on the evaluation tasks.

6 Conclusions

We propose a novel coarse-to-fine 3D manipulation policy, where tasks are decomposed and pretrained models are leveraged in the hierarchical architecture. Our method demonstrates strong generalization capabilities while maintaining the sample efficiency inherent to coarse-to-fine approaches. Although leveraging pre-trained models for robotics tasks is common, their effective adaptation for generalizable and precise is still under-explored. We hope this work inspires further research into building highly generalizable and sample-efficient 3D manipulation policies. Our method has two key limitations. First, key-frame based imitation learning is suitable for structured tasks that can be easily decomposed into discrete steps. Unstructured tasks, such as wiping a desk, where keyframes are difficult to define, present a significant challenge. Moreover, the current framework lacks a robust error-correction mechanism. An incorrect action prediction at any step might lead to task failure. A promising future direction is to integrate a self-correction module to enhance robustness. **LLM Usage** We used Deepseek (AI, 2024) and ChatGPT (OpenAI, 2024) for grammar check and related work retrieval. The authors have reviewed the content generated by the LLM.

Ethics Statement We adhere to the ICLR Code of Ethics and take full responsibility for the final content.

Reproducibility Statement To ensure reproducibility, we provide a comprehensive description of our method and experimental setup in the Section 4 and the Section 5, document all hyperparameters in the appendix Appendix A.2, and will release our code publicly upon acceptance.

REFERENCES

DeepSeek AI. Deepseek-v3. https://deepseek.com, 2024. Model and technical details available at https://github.com/deepseek-ai.

Shuai Bai, Keqin Chen, Xuejing Liu, Jialin Wang, Wenbin Ge, Sibo Song, Kai Dang, Peng Wang, Shijie Wang, Jun Tang, Humen Zhong, Yuanzhi Zhu, Mingkun Yang, Zhaohai Li, Jianqiang Wan, Pengfei Wang, Wei Ding, Zheren Fu, Yiheng Xu, Jiabo Ye, Xi Zhang, Tianbao Xie, Zesen Cheng, Hang Zhang, Zhibo Yang, Haiyang Xu, and Junyang Lin. Qwen2.5-vl technical report. *arXiv* preprint arXiv:2502.13923, 2025.

Lucas Beyer, Andreas Steiner, André Susano Pinto, Alexander Kolesnikov, Xiao Wang, Daniel Salz, Maxim Neumann, Ibrahim Alabdulmohsin, Michael Tschannen, Emanuele Bugliarello, Thomas Unterthiner, Daniel Keysers, Skanda Koppula, Fangyu Liu, Adam Grycner, Alexey Gritsenko, Neil Houlsby, Manoj Kumar, Keran Rong, Julian Eisenschlos, Rishabh Kabra, Matthias Bauer, Matko Bošnjak, Xi Chen, Matthias Minderer, Paul Voigtlaender, Ioana Bica, Ivana Balazevic, Joan Puigcerver, Pinelopi Papalampidi, Olivier Henaff, Xi Xiong, Radu Soricut, Jeremiah Harmsen, and Xiaohua Zhai. Paligemma: A versatile 3b vlm for transfer, 2024. URL https://arxiv.org/abs/2407.07726.

Anthony Brohan, Noah Brown, Justice Carbajal, Yevgen Chebotar, Xi Chen, Krzysztof Choromanski, Tianli Ding, Danny Driess, Avinava Dubey, Chelsea Finn, Pete Florence, Chuyuan Fu, Montse Gonzalez Arenas, Keerthana Gopalakrishnan, Kehang Han, Karol Hausman, Alex Herzog, Jasmine Hsu, Brian Ichter, Alex Irpan, Nikhil Joshi, Ryan Julian, Dmitry Kalashnikov, Yuheng Kuang, Isabel Leal, Lisa Lee, Tsang-Wei Edward Lee, Sergey Levine, Yao Lu, Henryk Michalewski, Igor Mordatch, Karl Pertsch, Kanishka Rao, Krista Reymann, Michael Ryoo, Grecia Salazar, Pannag Sanketi, Pierre Sermanet, Jaspiar Singh, Anikait Singh, Radu Soricut, Huong Tran, Vincent Vanhoucke, Quan Vuong, Ayzaan Wahid, Stefan Welker, Paul Wohlhart, Jialin Wu, Fei Xia, Ted Xiao, Peng Xu, Sichun Xu, Tianhe Yu, and Brianna Zitkovich. Rt-2: Vision-language-action models transfer web knowledge to robotic control. In *arXiv preprint arXiv:2307.15818*, 2023.

Chilam Cheang, Sijin Chen, Zhongren Cui, Yingdong Hu, Liqun Huang, Tao Kong, Hang Li, Yifeng Li, Yuxiao Liu, Xiao Ma, Hao Niu, Wenxuan Ou, Wanli Peng, Zeyu Ren, Haixin Shi, Jiawen Tian, Hongtao Wu, Xin Xiao, Yuyang Xiao, Jiafeng Xu, and Yichu Yang. Gr-3 technical report, 2025. URL https://arxiv.org/abs/2507.15493.

Shizhe Chen, Ricardo Garcia Pinel, Cordelia Schmid, and Ivan Laptev. Polarnet: 3d point clouds for language-guided robotic manipulation. In Jie Tan, Marc Toussaint, and Kourosh Darvish (eds.), *Proceedings of The 7th Conference on Robot Learning*, volume 229 of *Proceedings of Machine Learning Research*, pp. 1761–1781. PMLR, 06–09 Nov 2023. URL https://proceedings.mlr.press/v229/chen23b.html.

Danny Driess, Fei Xia, Mehdi S. M. Sajjadi, Corey Lynch, Aakanksha Chowdhery, Brian Ichter, Ayzaan Wahid, Jonathan Tompson, Quan Vuong, Tianhe Yu, Wenlong Huang, Yevgen Chebotar, Pierre Sermanet, Daniel Duckworth, Sergey Levine, Vincent Vanhoucke, Karol Hausman, Marc Toussaint, Klaus Greff, Andy Zeng, Igor Mordatch, and Pete Florence. PaLM-e: An embodied multimodal language model. In Andreas Krause, Emma Brunskill, Kyunghyun Cho, Barbara Engelhardt, Sivan Sabato, and Jonathan Scarlett (eds.), *Proceedings of the 40th International Conference on Machine Learning*, volume 202 of *Proceedings of Machine Learning Research*, pp.

```
8469-8488. PMLR, 23-29 Jul 2023. URL https://proceedings.mlr.press/v202/driess23a.html.
```

- Haoquan Fang, Markus Grotz, Wilbert Pumacay, Yi Ru Wang, Dieter Fox, Ranjay Krishna, and Jiafei Duan. Sam2act: Integrating visual foundation model with a memory architecture for robotic manipulation. In *Proceedings of the 42nd International Conference on Machine Learning*, 2025.
- Chongkai Gao, Zixuan Liu, Zhenghao Chi, Junshan Huang, Xin Fei, Yiwen Hou, Yuxuan Zhang, Yudi Lin, Zhirui Fang, Zeyu Jiang, and Lin Shao. Vla-os: Structuring and dissecting planning representations and paradigms in vision-language-action models. *arXiv preprint arXiv:2506.17561*, 2025. URL https://arxiv.org/abs/2506.17561.
- Ricardo Garcia, Shizhe Chen, and Cordelia Schmid. Towards generalizable vision-language robotic manipulation: A benchmark and llm-guided 3d policy. In *International Conference on Robotics and Automation (ICRA)*, 2025.
- Theophile Gervet, Zhou Xian, Nikolaos Gkanatsios, and Katerina Fragkiadaki. Act3d: 3d feature field transformers for multi-task robotic manipulation. In Jie Tan, Marc Toussaint, and Kourosh Darvish (eds.), *Proceedings of The 7th Conference on Robot Learning*, volume 229 of *Proceedings of Machine Learning Research*, pp. 3949–3965. PMLR, 06–09 Nov 2023. URL https://proceedings.mlr.press/v229/gervet23a.html.
- Ankit Goyal, Jie Xu, Yijie Guo, Valts Blukis, Yu-Wei Chao, and Dieter Fox. Rvt: Robotic view transformer for 3d object manipulation. In Jie Tan, Marc Toussaint, and Kourosh Darvish (eds.), Proceedings of The 7th Conference on Robot Learning, volume 229 of Proceedings of Machine Learning Research, pp. 694–710. PMLR, 06–09 Nov 2023. URL https://proceedings.mlr.press/v229/goyal23a.html.
- Ankit Goyal, Valts Blukis, Jie Xu, Yijie Guo, Yu-Wei Chao, and Dieter Fox. Rvt2: Learning precise manipulation from few demonstrations. *RSS*, 2024.
- Marcus Gualtieri and Robert Platt. Learning 6-dof grasping and pick-place using attention focus. In Aude Billard, Anca Dragan, Jan Peters, and Jun Morimoto (eds.), *Proceedings of The 2nd Conference on Robot Learning*, volume 87 of *Proceedings of Machine Learning Research*, pp. 477–486. PMLR, 29–31 Oct 2018. URL https://proceedings.mlr.press/v87/gualtieri18a.html.
- Marcus Gualtieri and Robert Platt. Learning manipulation skills via hierarchical spatial attention. *IEEE Transactions on Robotics*, 36(4):1067–1078, August 2020. ISSN 1941-0468. doi: 10.1109/tro.2020.2974093. URL http://dx.doi.org/10.1109/TRO.2020.2974093.
- Pierre-Louis Guhur, Shizhe Chen, Ricardo Garcia Pinel, Makarand Tapaswi, Ivan Laptev, and Cordelia Schmid. Instruction-driven history-aware policies for robotic manipulations. In Karen Liu, Dana Kulic, and Jeff Ichnowski (eds.), *Proceedings of The 6th Conference on Robot Learning*, volume 205 of *Proceedings of Machine Learning Research*, pp. 175–187. PMLR, 14–18 Dec 2023. URL https://proceedings.mlr.press/v205/guhur23a.html.
- Edward J Hu, yelong shen, Phillip Wallis, Zeyuan Allen-Zhu, Yuanzhi Li, Shean Wang, Lu Wang, and Weizhu Chen. LoRA: Low-rank adaptation of large language models. In *International Conference on Learning Representations*, 2022. URL https://openreview.net/forum?id=nZeVKeeFYf9.
- Physical Intelligence, Kevin Black, Noah Brown, James Darpinian, Karan Dhabalia, Danny Driess, Adnan Esmail, Michael Equi, Chelsea Finn, Niccolo Fusai, Manuel Y. Galliker, Dibya Ghosh, Lachy Groom, Karol Hausman, Brian Ichter, Szymon Jakubczak, Tim Jones, Liyiming Ke, Devin LeBlanc, Sergey Levine, Adrian Li-Bell, Mohith Mothukuri, Suraj Nair, Karl Pertsch, Allen Z. Ren, Lucy Xiaoyang Shi, Laura Smith, Jost Tobias Springenberg, Kyle Stachowicz, James Tanner, Quan Vuong, Homer Walke, Anna Walling, Haohuan Wang, Lili Yu, and Ury Zhilinsky. $\pi_{0.5}$: a vision-language-action model with open-world generalization, 2025. URL https://arxiv.org/abs/2504.16054.

- Stephen James, Kentaro Wada, Tristan Laidlow, and Andrew J. Davison. Coarse-to-fine q-attention: Efficient learning for visual robotic manipulation via discretisation. In 2022 IEEE/CVF Conference on Computer Vision and Pattern Recognition (CVPR), pp. 13729–13738, 2022. doi: 10.1109/CVPR52688.2022.01337.
- Yueru Jia, Jiaming Liu, Sixiang Chen, Chenyang Gu, Zhilve Wang, Longzan Luo, Xiaoqi Li, Pengwei Wang, Zhongyuan Wang, Renrui Zhang, and Shanghang Zhang. Lift3d policy: Lifting 2d foundation models for robust 3d robotic manipulation. In *Proceedings of the IEEE/CVF Conference on Computer Vision and Pattern Recognition (CVPR)*, pp. 17347–17358, June 2025.
- Edward Johns. Coarse-to-fine imitation learning: Robot manipulation from a single demonstration. In *IEEE International Conference on Robotics and Automation (ICRA)*, 2021.
- Tsung-Wei Ke, Nikolaos Gkanatsios, and Katerina Fragkiadaki. 3d diffuser actor: Policy diffusion with 3d scene representations, 2024. URL https://arxiv.org/abs/2402.10885.
- Moo Jin Kim, Karl Pertsch, Siddharth Karamcheti, Ted Xiao, Ashwin Balakrishna, Suraj Nair, Rafael Rafailov, Ethan Foster, Grace Lam, Pannag Sanketi, Quan Vuong, Thomas Kollar, Benjamin Burchfiel, Russ Tedrake, Dorsa Sadigh, Sergey Levine, Percy Liang, and Chelsea Finn. Openvla: An open-source vision-language-action model. *arXiv preprint arXiv:2406.09246*, 2024.
- Chengmeng Li, Junjie Wen, Yan Peng, Yaxin Peng, Feifei Feng, and Yichen Zhu. Pointvla: Injecting the 3d world into vision-language-action models, 2025a. URL https://arxiv.org/abs/2503.07511.
- Peiyan Li, Yixiang Chen, Hongtao Wu, Xiao Ma, Xiangnan Wu, Yan Huang, Liang Wang, Tao Kong, and Tieniu Tan. Bridgevla: Input-output alignment for efficient 3d manipulation learning with vision-language models, 2025b. URL https://arxiv.org/abs/2506.07961.
- Qixiu Li, Yaobo Liang, Zeyu Wang, Lin Luo, Xi Chen, Mozheng Liao, Fangyun Wei, Yu Deng, Sicheng Xu, Yizhong Zhang, et al. Cogact: A foundational vision-language-action model for synergizing cognition and action in robotic manipulation. *arXiv* preprint arXiv:2411.19650, 2024.
- Suhan Ling, Yian Wang, Ruihai Wu, Shiguang Wu, Yuzheng Zhuang, Tianyi Xu, Yu Li, Chang Liu, and Hao Dong. Articulated object manipulation with coarse-to-fine affordance for mitigating the effect of point cloud noise. In *2024 IEEE International Conference on Robotics and Automation (ICRA)*, pp. 10895–10901, 2024. doi: 10.1109/ICRA57147.2024.10610593.
- Songming Liu, Lingxuan Wu, Bangguo Li, Hengkai Tan, Huayu Chen, Zhengyi Wang, Ke Xu, Hang Su, and Jun Zhu. Rdt-1b: a diffusion foundation model for bimanual manipulation. *International Conference on Learning Representations (ICLR)*, 2024.
- Yangjun Liu, Sheng Liu, Binghan Chen, Zhi-Xin Yang, and Sheng Xu. Fusion-perception-to-action transformer: Enhancing robotic manipulation with 3-d visual fusion attention and proprioception. *IEEE Transactions on Robotics*, 41:1553–1567, 2025. doi: 10.1109/TRO.2025.3539193.
- Yao Mu, Qinglong Zhang, Mengkang Hu, Wenhai Wang, Mingyu Ding, Jun Jin, Bin Wang, Jifeng Dai, Yu Qiao, and Ping Luo. EmbodiedGPT: Vision-language pre-training via embodied chain of thought. In *Thirty-seventh Conference on Neural Information Processing Systems*, 2023. URL https://openreview.net/forum?id=IL5zJqfxAa.
- NVIDIA, Johan Bjorck, Fernando Castañeda, Nikita Cherniadev, Xingye Da, Runyu Ding, Linxi "Jim" Fan, Yu Fang, Dieter Fox, Fengyuan Hu, Spencer Huang, Joel Jang, Zhenyu Jiang, Jan Kautz, Kaushil Kundalia, Lawrence Lao, Zhiqi Li, Zongyu Lin, Kevin Lin, Guilin Liu, Edith Llontop, Loic Magne, Ajay Mandlekar, Avnish Narayan, Soroush Nasiriany, Scott Reed, You Liang Tan, Guanzhi Wang, Zu Wang, Jing Wang, Qi Wang, Jiannan Xiang, Yuqi Xie, Yinzhen Xu, Zhenjia Xu, Seonghyeon Ye, Zhiding Yu, Ao Zhang, Hao Zhang, Yizhou Zhao, Ruijie Zheng, and Yuke Zhu. Gr00t n1: An open foundation model for generalist humanoid robots, 2025. URL https://arxiv.org/abs/2503.14734.
- Octo Model Team, Dibya Ghosh, Homer Walke, Karl Pertsch, Kevin Black, Oier Mees, Sudeep Dasari, Joey Hejna, Charles Xu, Jianlan Luo, Tobias Kreiman, You Liang Tan, Lawrence Yunliang Chen, Pannag Sanketi, Quan Vuong, Ted Xiao, Dorsa Sadigh, Chelsea Finn, and Sergey Levine.

Octo: An open-source generalist robot policy. In *Proceedings of Robotics: Science and Systems*, Delft, Netherlands, 2024.

OpenAI. Chatgpt-4o (may 13, 2024 version) [large language model]. https://chat.openai.com, 2024.

Maxime Oquab, Timothée Darcet, Théo Moutakanni, Huy Q. Vo, Marc Szafraniec, Vasil Khalidov, Pierre Fernandez, Daniel Haziza, Francisco Massa, Alaaeldin El-Nouby, Mahmoud Assran, Nicolas Ballas, Wojciech Galuba, Russ Howes, Po-Yao (Bernie) Huang, Shang-Wen Li, Ishan Misra, Michael G. Rabbat, Vasu Sharma, Gabriel Synnaeve, Huijiao Xu, Hervé Jégou, Julien Mairal, Patrick Labatut, Armand Joulin, and Piotr Bojanowski. Dinov2: Learning robust visual features without supervision. *ArXiv*, abs/2304.07193, 2023. URL https://api.semanticscholar.org/CorpusID:258170077.

Delin Qu, Haoming Song, Qizhi Chen, Yuanqi Yao, Xinyi Ye, Yan Ding, Zhigang Wang, JiaYuan Gu, Bin Zhao, Dong Wang, and Xuelong Li. Spatialvla: Exploring spatial representations for visual-language-action model, 2025. URL https://arxiv.org/abs/2501.15830.

Nikhila Ravi, Valentin Gabeur, Yuan-Ting Hu, Ronghang Hu, Chaitanya Ryali, Tengyu Ma, Haitham Khedr, Roman Rädle, Chloe Rolland, Laura Gustafson, Eric Mintun, Junting Pan, Kalyan Vasudev Alwala, Nicolas Carion, Chao-Yuan Wu, Ross Girshick, Piotr Dollár, and Christoph Feichtenhofer. Sam 2: Segment anything in images and videos, 2024. URL https://arxiv.org/abs/2408.00714.

Mohit Shridhar, Lucas Manuelli, and Dieter Fox. Perceiver-actor: A multi-task transformer for robotic manipulation. In *Proceedings of the 6th Conference on Robot Learning (CoRL)*, 2022.

Mustafa Shukor, Dana Aubakirova, Francesco Capuano, Pepijn Kooijmans, Steven Palma, Adil Zouitine, Michel Aractingi, Caroline Pascal, Martino Russi, Andres Marafioti, Simon Alibert, Matthieu Cord, Thomas Wolf, and Remi Cadene. Smolvla: A vision-language-action model for affordable and efficient robotics, 2025. URL https://arxiv.org/abs/2506.01844.

Gemini Robotics Team, Saminda Abeyruwan, Joshua Ainslie, Jean-Baptiste Alayrac, Montserrat Gonzalez Arenas, Travis Armstrong, Ashwin Balakrishna, Robert Baruch, Maria Bauza, Michiel Blokzijl, Steven Bohez, Konstantinos Bousmalis, Anthony Brohan, Thomas Buschmann, Arunkumar Byravan, Serkan Cabi, Ken Caluwaerts, Federico Casarini, Oscar Chang, Jose Enrique Chen, Xi Chen, Hao-Tien Lewis Chiang, Krzysztof Choromanski, David D'Ambrosio, Sudeep Dasari, Todor Davchev, Coline Devin, Norman Di Palo, Tianli Ding, Adil Dostmohamed, Danny Driess, Yilun Du, Debidatta Dwibedi, Michael Elabd, Claudio Fantacci, Cody Fong, Erik Frey, Chuyuan Fu, Marissa Giustina, Keerthana Gopalakrishnan, Laura Graesser, Leonard Hasenclever, Nicolas Heess, Brandon Hernaez, Alexander Herzog, R. Alex Hofer, Jan Humplik, Atil Iscen, Mithun George Jacob, Deepali Jain, Ryan Julian, Dmitry Kalashnikov, M. Emre Karagozler, Stefani Karp, Chase Kew, Jerad Kirkland, Sean Kirmani, Yuheng Kuang, Thomas Lampe, Antoine Laurens, Isabel Leal, Alex X. Lee, Tsang-Wei Edward Lee, Jacky Liang, Yixin Lin, Sharath Maddineni, Anirudha Majumdar, Assaf Hurwitz Michaely, Robert Moreno, Michael Neunert, Francesco Nori, Carolina Parada, Emilio Parisotto, Peter Pastor, Acorn Pooley, Kanishka Rao, Krista Reymann, Dorsa Sadigh, Stefano Saliceti, Pannag Sanketi, Pierre Sermanet, Dhruv Shah, Mohit Sharma, Kathryn Shea, Charles Shu, Vikas Sindhwani, Sumeet Singh, Radu Soricut, Jost Tobias Springenberg, Rachel Sterneck, Razvan Surdulescu, Jie Tan, Jonathan Tompson, Vincent Vanhoucke, Jake Varley, Grace Vesom, Giulia Vezzani, Oriol Vinyals, Ayzaan Wahid, Stefan Welker, Paul Wohlhart, Fei Xia, Ted Xiao, Annie Xie, Jinyu Xie, Peng Xu, Sichun Xu, Ying Xu, Zhuo Xu, Yuxiang Yang, Rui Yao, Sergey Yaroshenko, Wenhao Yu, Wentao Yuan, Jingwei Zhang, Tingnan Zhang, Allan Zhou, and Yuxiang Zhou. Gemini robotics: Bringing ai into the physical world, 2025. URL https://arxiv.org/abs/2503.20020.

Chenxi Wang, Hongjie Fang, Haoshu Fang, and Cewu Lu. Rise: 3d perception makes real-world robot imitation simple and effective. 2024 IEEE/RSJ International Conference on Intelligent Robots and Systems (IROS), pp. 2870–2877, 2024a. URL https://api.semanticscholar.org/CorpusID:269214333.

Yixuan Wang, Guang Yin, Binghao Huang, Tarik Kelestemur, Jiuguang Wang, and Yunzhu Li. Gendp: 3d semantic fields for category-level generalizable diffusion policy. In 8th Annual Conference on Robot Learning, 2024b.

- Junjie Wen, Yichen Zhu, Jinming Li, Minjie Zhu, Kun Wu, Zhiyuan Xu, Ning Liu, Ran Cheng, Chaomin Shen, Yaxin Peng, et al. Tinyvla: Towards fast, data-efficient vision-language-action models for robotic manipulation. In *IEEE Robotics and Automation Letters (RA-L)*, 2025a.
- Junjie Wen, Yichen Zhu, Zhibing Tang, Jinming Li, Yaxin Peng, Chaomin Shen, and Feifei Feng. Dexvla: Vision-language model with plug-in diffusion expert for visuomotor policy learning. *Conference on Robot Learning (CoRL)*, 2025b.
- Wentao Yuan, Jiafei Duan, Valts Blukis, Wilbert Pumacay, Ranjay Krishna, Adithyavairavan Murali, Arsalan Mousavian, and Dieter Fox. Robopoint: A vision-language model for spatial affordance prediction in robotics. In 8th Annual Conference on Robot Learning, 2024. URL https://openreview.net/forum?id=GVX6jpZOhU.
- Michał Zawalski, William Chen, Karl Pertsch, Oier Mees, Chelsea Finn, and Sergey Levine. Robotic control via embodied chain-of-thought reasoning. In 8th Annual Conference on Robot Learning, 2024. URL https://openreview.net/forum?id=S70MgnIA0v.
- Yanjie Ze, Gu Zhang, Kangning Zhang, Chenyuan Hu, Muhan Wang, and Huazhe Xu. 3d diffusion policy: Generalizable visuomotor policy learning via simple 3d representations. In *Proceedings of Robotics: Science and Systems (RSS)*, 2024.
- Xiaohua Zhai, Basil Mustafa, Alexander Kolesnikov, and Lucas Beyer. Sigmoid loss for language image pre-training. 2023 IEEE/CVF International Conference on Computer Vision (ICCV), pp. 11941–11952, 2023. URL https://api.semanticscholar.org/CorpusID: 257767223.
- Qingqing Zhao, Yao Lu, Moo Jin Kim, Zipeng Fu, Zhuoyang Zhang, Yecheng Wu, Zhaoshuo Li, Qianli Ma, Song Han, Chelsea Finn, Ankur Handa, Ming-Yu Liu, Donglai Xiang, Gordon Wetzstein, and Tsung-Yi Lin. Cot-vla: Visual chain-of-thought reasoning for vision-language-action models. 2025 IEEE/CVF Conference on Computer Vision and Pattern Recognition (CVPR), pp. 1702–1713, 2025. URL https://api.semanticscholar.org/CorpusID:277435005.
- Haoyu Zhen, Xiaowen Qiu, Peihao Chen, Jincheng Yang, Xin Yan, Yilun Du, Yining Hong, and Chuang Gan. 3d-vla: a 3d vision-language-action generative world model. In *Proceedings of the 41st International Conference on Machine Learning*, ICML'24. JMLR.org, 2024.
- Haoyi Zhu, Honghui Yang, Yating Wang, Jiange Yang, Limin Wang, and Tong He. Spa: 3d spatial-awareness enables effective embodied representation. In Y. Yue, A. Garg, N. Peng, F. Sha, and R. Yu (eds.), *International Conference on Representation Learning*, volume 2025, pp. 26361–26391, 2025. URL https://proceedings.iclr.cc/paper_files/paper/2025/file/421fcf51a0e243f15f977553a6f482cb-Paper-Conference.pdf.

Table 4: **Training and evaluation tasks & variations in GemBench.** The evaluation tasks contain four levels of generalization, where Level 1 evaluates the generalization to novel placements, Level 2 novel rigid objects, Level 3 novel articulated objects, and Level 4 novel long-horizon tasks.

	Train / l		Level		I	Level 3		Level 4
	Task	Variation	Color	Shape	Instance	Category	Action-Part	Long-horizon
Press	Push button	maroon button navy button yellow button	azure button rose button white button	Lamp on				2 buttons 3 buttons 4 buttons
Pick	Pick and lift	red block lime block cyan block magenta cup	teal block violet block black block	red cylinder red star red moon				
	Pick up cup	silver cup orange cup	gray cup olive cup purple cup	red toy				
Push	Slide block	green target blue target	pink target yellow target					
T usii	Reach and drag	teal target black target	cyan target navy target					
Screw	Close jar	azure jar violet jar	blue jar green jar					
Serew	Screw bulb	rose bulb white bulb	lime bulb maroon bulb					
Close	Close fridge Close laptop lid Close microwave	fridge laptop lid microwave			fridge2 laptop lid2 microwave2	grill	door box drawer	
Open	Open door Open box Open drawer	door box bottom drawer top drawer			door2 box2 drawer2, drawer3 long drawer w/ 4 levels	toilet	fridge laptop lid microwave middle drawer	Take shoes out of box Put 3 items in drawer
	Stack blocks	2 gray blocks 2 olive blocks 2 purple blocks	2 orange blocks 2 silver blocks 2 magenta blocks		- V			Stack 3-4 blocks Stack 2 cups
Put/ Stack	Put groceries	crackers box soup can		mustard bottle sugar box				Put all groceries
	Put money	bottom shelf middle shelf		Put cube in bottom shelf			top shelf	

Table 5: **Training time and hyperparameters used in different experiments.** Here we list the training time and hyperparameters used for training the model with GemBench and real-world data.

		GemBench		Real-world
	Coarse task planner	Fine-grained Action Predictor	Coarse task planner	Fine-grained Action Predictor
Training time	6 hours	3 hours	1 hour	1 hour
Learning rata	3e-4	0.0024	1e-4	0.0024
Batch Size	64	192	64	192
Epochs	1	5	1	3
Lora Rank	8	/	8	/
Lora Alpha	32	/	32	/
Freeze Vit	False	/	False	/
Freeze Aligner	True	/	True	/
Freeze LLM	False	/	False	/

A APPENDIX

A.1 GEMBENCH TASK SPECIFICATION

The detailed tasks and variations in GemBench (Garcia et al., 2025) used for training and evaluation are listed in Table 4.

A.2 EXPERIMENTAL DETAILS

All experiments are conducted on 4 NVIDIA RTX 4090 GPU. The hyperparameters and training time are listed in Appendix A.2.

A.3 GEMBENCH SUCCESS RATE PER TASK

The results for each task across different generalization levels in Gembench are listed in Table 6, Table 7, Table 8, Table 9.

Method	Avg.	Close Fridge+0	Close Jar+15	Close Jar+16	CloseLaptop Lid+0	Close Microwave+0	LightBulb In+17	LightBulb In+19	Open Box+0	Open Door+0	Open Drawer+0
HiveFormer (Guhur et al., 2023)	60.3+1.5	96+4 2	64+13.9	92 _{±2.7}	90 _{±3.5}	88+76	12±4.5	13+6.7	4+42	53±15.2	15±12.2
PolarNet (Chen et al., 2023)	$77.6_{\pm0.9}$	$99_{\pm 2.2}$	99 _{±2.2}	99 _{±2.2}	95±3.5	98±2.7	$72_{\pm 12.5}$	71 _{±6.5}	32±11.5	$69_{\pm 8.9}$	$61_{\pm 12.4}$
3D Diffuser Actor (Ke et al., 2024)	$91.9_{\pm 0.8}$	$100_{\pm 0.0}$	$100_{\pm 0.0}$	$100_{\pm 0.0}$	99 _{±2.2}	$100_{\pm 0.0}$	$85_{\pm 5.0}$	$88_{\pm 2.7}$	$11_{\pm 2.2}$	$96_{\pm 4.2}$	$82_{\pm 9.1}$
RVT2 (Goyal et al., 2024)	$89.0_{\pm0.8}$	$77_{\pm 11.0}$	$97_{\pm 4.5}$	$98_{\pm 2.7}$	$77_{\pm 13.0}$	$100_{\pm 0.0}$	$93_{\pm 5.7}$	$91_{\pm 8.2}$	$7_{\pm 4.5}$	$98_{\pm 4.5}$	93±5.7
3D-LOTUS (Garcia et al., 2025)	94.3 _{±3.5}	$96_{\pm 3.7}$	$100_{\pm 0.0}$	$100_{\pm 0.0}$	98±2.5	$98_{\pm 4.0}$	$84_{\pm 7.4}$	85±9.5	$99_{\pm 2.0}$	77 _{±2.5}	83±8.7
3D-LOTUS++ (Garcia et al., 2025)	$68.7_{\pm 0.6}$	$95_{\pm 0.0}$	$100_{\pm 0.0}$	$99_{\pm 2.0}$	$28_{\pm 2.5}$	87 _{±5.1}	$55_{\pm 10.5}$	$45_{\pm 8.9}$	55±8.9	$79_{\pm 9.7}$	$68_{\pm 12.5}$
BridgeVLA (Li et al., 2025b)	$91.1_{\pm 1.1}$	$99_{\pm 2.0}$	$98_{\pm 4.0}$	$100_{\pm 0.0}$	$97_{\pm 2.5}$	85±5.5	$90_{\pm 5.5}$	$87_{\pm 7.5}$	$76_{\pm 10.2}$	$70_{\pm 12.3}$	$86_{\pm 5.8}$
CLAP	$83.9_{\pm0.3}$	$88_{\pm 4.5}$	$98_{\pm 2.7}$	$100_{\pm 0.0}$	$88_{\pm 9.1}$	$99_{\pm 2.2}$	$84_{\pm 6.5}$	$76_{\pm 9.1}$	$17_{\pm 5.7}$	$82_{\pm 4.5}$	$87_{\pm 13.0}$
	Open	Pick&	Pick&	Pick&	PickUp	PickUp	PickUp	Push	Push	Push	PutIn
Method	Drawer+2	Lift+0	Lift+2	Lift+7	Cup+8	Cup+9	Cup+11	Button+0	Button+3	Button+4	Cupboard+0
HiveFormer (Guhur et al., 2023)	59+74	86+4 2	92+67	93+27	83 _{±7.6}	69 _{±12.9}	61 _{±19.8}	84±11.9	68+6.7	87+76	34+8 2
PolarNet (Chen et al., 2023)	$90_{\pm 7.1}$	$92_{\pm 9.1}$	$84_{\pm 7.4}$	$88_{\pm 5.7}$	82 _{±7.6}	$79_{\pm 4.2}$	$72_{\pm 10.4}$	$100_{\pm 0.0}$	$100_{\pm 0.0}$	$99_{\pm 2.2}$	52±7.6
3D Diffuser Actor (Ke et al., 2024)	$97_{\pm 4.5}$	$99_{\pm 2.2}$	$99_{\pm 2.2}$	$99_{\pm 2.2}$	$96_{\pm 2.2}$	97 _{±4.5}	$98_{\pm 2.7}$	$98_{\pm 2.7}$	$96_{\pm 4.2}$	98±2.7	85±5.0
RVT2 (Goyal et al., 2024)	$94_{\pm 4.2}$	$99_{\pm 2.2}$	$98_{\pm 2.7}$	$100_{\pm 0.0}$	$99_{\pm 2.2}$	$99_{\pm 2.2}$	$99_{\pm 2.2}$	$100_{\pm 0.0}$	$100_{\pm 0.0}$	$100_{\pm 0.0}$	$88_{\pm 8.4}$
3D-LOTUS (Garcia et al., 2025)	$93_{\pm 6.0}$	$99_{\pm 2.0}$	$100_{\pm 0.0}$	$99_{\pm 2.0}$	$97_{\pm 4.0}$	$96_{\pm 3.7}$	$94_{\pm 4.9}$	$99_{\pm 2.0}$	$99_{\pm 2.0}$	$100_{\pm 0.0}$	89 _{±5.8}
3D-LOTUS++ (Garcia et al., 2025)	$75_{\pm 4.5}$	$97_{\pm 6.0}$	$94_{\pm 3.7}$	$93_{\pm 5.1}$	$86_{\pm 8.0}$	88±6.8	$91_{\pm 4.9}$	$100_{\pm 0.0}$	$100_{\pm 0.0}$	$100_{\pm 0.0}$	$1_{\pm 2.0}$
BridgeVLA (Li et al., 2025b)	$99_{\pm 2.0}$	$99_{\pm 2.0}$	$100_{\pm 0.0}$	$98_{\pm 2.5}$	$96_{\pm 2.0}$	$94_{\pm 3.7}$	$99_{\pm 2.0}$	$100_{\pm 0.0}$	$98_{\pm 4.0}$	$98_{\pm 4.0}$	$74_{\pm 6.6}$
CLAP	$98_{\pm 2.7}$	$98_{\pm 2.7}$	$99_{\pm 2.2}$	$99_{\pm 2.2}$	$94_{\pm 5.5}$	$99_{\pm 2.2}$	$93_{\pm 7.6}$	$100_{\pm 0.0}$	$100_{\pm 0.0}$	$97_{\pm 2.7}$	$58_{\pm 10.4}$
Method	PutIn Cupboard+3	PutMoney InSafe+0	PutMoney InSafe+1	Reach& Drag+14	Reach& Drag+18	Slide Block+0	Slide Block+1	Stack Blocks+30	Stack Blocks+36	Stack Blocks+39	
HiveFormer (Guhur et al., 2023)	$74_{\pm 6.5}$	$85_{\pm 3.5}$	$88_{\pm 2.7}$	$37_{\pm 5.7}$	$32_{\pm 7.6}$	$99_{\pm 2.2}$	$91_{\pm 12.4}$	$6_{\pm 5.5}$	$7_{\pm 4.5}$	$6_{\pm 4.2}$	
PolarNet (Chen et al., 2023)	$88_{\pm 4.5}$	$93_{\pm 4.5}$	$95_{\pm 5.0}$	$99_{\pm 2.2}$	$99_{\pm 2.2}$	$100_{\pm 0.0}$	$0_{\pm 0.0}$	$34_{\pm 10.8}$	$30_{\pm 9.4}$	$36_{\pm 12.9}$	
3D Diffuser Actor (Ke et al., 2024)	$82_{\pm 11.5}$	$95_{\pm 5.0}$	$98_{\pm 2.7}$	$100_{\pm 0.0}$	$99_{\pm 2.2}$	$100_{\pm 0.0}$	$89_{\pm 4.2}$	$88_{\pm 7.6}$	$85_{\pm 6.1}$	$89_{\pm 5.5}$	
RVT2 (Goyal et al., 2024)	$80_{\pm 6.1}$	$93_{\pm 8.4}$	$96_{\pm 8.5}$	$85_{\pm 10.0}$	$94_{\pm 2.2}$	$100_{\pm 0.0}$	$37_{\pm 6.7}$	$88_{\pm 5.7}$	$93_{\pm 2.7}$	$88_{\pm 11.5}$	
3D-LOTUS (Garcia et al., 2025)	$72_{\pm 11.2}$	$94_{\pm 3.7}$	$99_{\pm 2.0}$	$99_{\pm 2.0}$	$100_{\pm 0.0}$	$100_{\pm 0.0}$	$100_{\pm 0.0}$	$94_{\pm 5.8}$	$91_{\pm 6.6}$	$90_{\pm 4.5}$	
3D-LOTUS++ (Garcia et al., 2025)	$2_{\pm 2.5}$	$22_{\pm 6.8}$	$16_{\pm 4.9}$	$94_{\pm 3.7}$	$62_{\pm 8.7}$	$100_{\pm 0.0}$	$65_{\pm 5.5}$	$86_{\pm 5.8}$	$20_{\pm 4.5}$	$28_{\pm 13.6}$	
BridgeVLA (Li et al., 2025b)	$84_{\pm 6.6}$	$79_{\pm 9.7}$	$86_{\pm 3.7}$	$96_{\pm 5.8}$	$97_{\pm 4.0}$	$100_{\pm 0.0}$	$90_{\pm 5.5}$	$77_{\pm 8.1}$	$87_{\pm 4.0}$	$85_{\pm 7.8}$	
CLAP	$69_{\pm 12.4}$	$80_{\pm 6.1}$	82 _{±7.6}	$90_{\pm 3.5}$	$90_{\pm 34.5}$	55 _{±5.0}	$5_{\pm 5.0}$	$96_{\pm 4.2}$	$85_{\pm 3.5}$	$90_{\pm 6.1}$	

Table 6: Per-task Success Rate on GemBench Level 1.

Method	Avg.	Push Button+13	Push Button+15	Push Button+17	Pick& Lift+14	Pick& Lift+16	Pick& Lift+18	PickUp Cup+10	PickUp Cup+12	PickUp Cup+13
HiveFormer (Guhur et al., 2023)	26.1+1.4	97 _{±2.7}	85+10.0	88+2.7	21 _{±6.5}	$9_{\pm 4.2}$	8+6.7	30+7.1	22±13.5	26±10.6
PolarNet (Chen et al., 2023)	$37.1_{\pm 1.4}$	$100_{\pm 0.0}$	$100_{\pm 0.0}$	85±7.9	$3_{\pm 4.5}$	1 _{±2.2}	$0_{\pm 0.0}$	$48_{\pm 11.0}$	46±8.9	$16_{\pm 6.5}$
3D Diffuser Actor (Ke et al., 2024)	43.4+2.8	$87_{+13.0}$	81+6.5	$60_{+9.4}$	$9_{\pm 4.2}$	$18_{\pm 9.1}$	$0_{\pm 0.0}$	84+5.5	$60_{+11.7}$	$62_{\pm 13.0}$
RVT2 (Goyal et al., 2024)	$51.0_{\pm 2.3}$	$100_{\pm 0.0}$	$100_{\pm 0.0}$	$100_{\pm 0.0}$	$47_{\pm 7.6}$	29 _{±9.6}	8±4.5	81 _{±8.2}	59 _{±9.6}	$72_{\pm 9.7}$
3D-LOTUS (Garcia et al., 2025)	$49.9_{\pm 2.2}$	$99_{\pm 2.0}$	$100_{\pm 0.0}$	$100_{\pm 0.0}$	$3_{\pm 2.5}$	$18_{\pm 8.7}$	$33_{\pm 9.3}$	$89_{\pm 3.7}$	$78_{\pm 8.7}$	$57_{\pm 7.5}$
3D-LOTUS++ (Garcia et al., 2025)	$64.5_{\pm 0.9}$	$99_{\pm 2.0}$	$100_{\pm 0.0}$	$99_{\pm 2.0}$	$94_{\pm 3.7}$	$96_{\pm 3.7}$	$95_{\pm 3.2}$	$79_{\pm 4.9}$	$89_{\pm 9.7}$	$84_{\pm 10.2}$
BridgeVLA (Li et al., 2025b)	$65.0_{\pm 1.3}$	$100_{\pm 0.0}$	$100_{\pm 0.0}$	$100_{\pm 0.0}$	$74_{\pm 9.7}$	$89_{\pm 4.9}$	$0_{\pm 0.0}$	$91_{\pm 3.7}$	$90_{\pm 3.2}$	$90_{\pm 6.3}$
CLAP	$83.2_{\pm 1.9}$	$100_{\pm 0.0}$	$100_{\pm 0.0}$	$100_{\pm 0.0}$	$99_{\pm 2.2}$	$100_{\pm 0.0}$	$98_{\pm 2.7}$	$93_{\pm 4.5}$	$97_{\pm 2.7}$	$98_{\pm 2.7}$
	Stack	Stack	Stack	Slide	Slide	Close	Close	LightBulb	LightBulb	Lamp
Method	Blocks+24	Blocks+27	Blocks+33	Block+2	Block+3	Jar+3	Jar+4	In+1	In+2	On+0
HiveFormer (Guhur et al., 2023)	0+0.0	$4_{\pm 4.2}$	$0_{\pm 0.0}$	$0_{\pm 0.0}$	$0_{\pm 0.0}$	$0_{\pm 0.0}$	$0_{\pm 0.0}$	4+4.2	0+0.0	7 _{±4.5}
PolarNet (Chen et al., 2023)	$1_{\pm 2.2}$	$2_{\pm 2.7}$	$6_{\pm 8.2}$	$0_{\pm 0.0}$	$0_{\pm 0.0}$	$20_{\pm 10.6}$	$82_{\pm 5.7}$	$22_{\pm 11.5}$	$17_{\pm 8.4}$	$14_{\pm 10.8}$
3D Diffuser Actor (Ke et al., 2024)	$66_{\pm 13.9}$	$82_{\pm 2.7}$	$50_{\pm 14.6}$	$0_{\pm 0.0}$	$0_{\pm 0.0}$	$23_{\pm 16.8}$	$82_{\pm 5.7}$	$51_{\pm 17.8}$	$60_{\pm 10.0}$	$7_{\pm 7.6}$
RVT2 (Goyal et al., 2024)	$18_{\pm 4.5}$	$56_{\pm 16.7}$	$45_{\pm 13.7}$	$0_{\pm 0.0}$	$1_{\pm 2.2}$	$7_{\pm 7.6}$	$77_{\pm 5.7}$	$68_{\pm 14.4}$	$6_{\pm 6.5}$	$0_{\pm 0.0}$
3D-LOTUS (Garcia et al., 2025)	$13_{\pm 8.1}$	$40_{\pm 9.5}$	$69_{\pm 5.8}$	$0_{\pm 0.0}$	$0_{\pm 0.0}$	$71_{\pm 5.8}$	$90_{\pm 4.5}$	$24_{\pm 4.9}$	$41_{\pm 8.6}$	$0_{\pm 0.0}$
3D-LOTUS++ (Garcia et al., 2025)	$22_{\pm 9.3}$	$83_{\pm 7.5}$	$59_{\pm 3.7}$	$27_{\pm 9.8}$	$5_{\pm 3.2}$	$98_{\pm 2.5}$	$96_{\pm 3.7}$	$56_{\pm 9.7}$	$43_{\pm 7.5}$	$2_{\pm 2.0}$
BridgeVLA (Li et al., 2025b)	$61_{\pm 10.7}$	$51_{\pm 13.2}$	$79_{\pm 8.6}$	$12_{\pm 9.3}$	$3_{\pm 4.0}$	$66_{\pm 6.6}$	$88_{\pm 4.0}$	$66_{\pm 8.6}$	$74_{\pm 5.8}$	$7_{\pm 4.0}$
CLAP	$95_{\pm 3.5}$	$86_{\pm 2.2}$	$91_{\pm 4.2}$	$18_{\pm 5.7}$	$68_{\pm 5.7}$	$95_{\pm 3.5}$	$98_{\pm 4.5}$	$66_{\pm 5.5}$	$81_{\pm 6.5}$	$20_{\pm 6.1}$
Method	Reach& Drag+5	Reach& Drag+7	PutCube InSafe+0	Pick&Lift Cylinder+0	Pick&Lift Star+0	Pick&Lift Moon+0	Pick&Lift Toy+0	PutIn Cupboard+7	PutIn Cupboard+8	
W F (G) 1 2000							•			
HiveFormer (Guhur et al., 2023)	1 _{±2.2}	$0_{\pm 0.0}$	4 _{±2.2}	78 _{±5.7}	73 _{±7.6}	88 _{±2.7}	87 _{±4.5}	$0_{\pm 0.0}$	$0_{\pm 0.0}$	
PolarNet (Chen et al., 2023)	61±8.2	10 _{±6.1}	$40_{\pm 14.1}$	93 _{±6.7}	88 _{±8.4}	$93_{\pm 6.7}$	$90_{\pm 3.5}$	$0_{\pm 0.0}$	$0_{\pm 0.0}$	
3D Diffuser Actor (Ke et al., 2024)	$0_{\pm 0.0}$	$64_{\pm 6.5}$	3 _{±2.7}	99 _{±2.2}	43 _{±17.9}	91 _{±9.6}	$30_{\pm 9.4}$	$0_{\pm 0.0}$	3 _{±4.5}	
RVT2 (Goyal et al., 2024)	91 _{±2.2}	89 _{±6.5}	6±5.5	98 _{±2.7}	98 _{±4.5}	$94_{\pm 4.2}$	78 _{±8.4}	$0_{\pm 0.0}$	$0_{\pm 0.0}$	
3D-LOTUS (Garcia et al., 2025)	95±4.5	18±10.8	25±5.5	88 _{±8.7}	69 _{±6.6}	$80_{\pm 8.4}$	96±3.7	$0_{\pm 0.0}$	$0_{\pm 0.0}$	
3D-LOTUS++ (Garcia et al., 2025)	$94_{\pm 2.0}$	$64_{\pm 12.4}$	37 _{±5.1}	91 _{±2.0}	$94_{\pm 3.7}$	29 _{±6.6}	71 _{±2.0}	$1_{\pm 2.0}$	$0_{\pm 0.0}$	
BridgeVLA (Li et al., 2025b)	94±3.7	96±3.7	3±2.5	98 _{±2.5}	99 _{±2.0}	95±3.2	93 _{±5.1}	$0_{\pm 0.0}$	0 _{±0.0}	
CLAP	$95_{\pm 3.5}$	$90_{\pm 6.1}$	$61_{\pm 14.7}$	$97_{\pm 2.7}$	$100_{\pm 0.0}$	$98_{\pm 2.7}$	$84_{\pm 8.2}$	$50_{\pm 11.2}$	$53_{\pm 12.5}$	

Table 7: Per-task Success Rate on GemBench Level 2.

A.4 REAL-WORLD EXPERIMENTS

An overview of the tasks used in real-world experiments are shown in Figure 4.

Method	Avg.	Close Door+0	Close Box+0	Close Fridge2+0	CloseLaptop Lid2+0	Close Microwave2+0	Open Door2+0	Open Box2+0
HiveFormer (Guhur et al., 2023)	35.1 _{±1.7}	$0_{\pm 0.0}$	1 _{±2.2}	34+9.6	52±9.1	15±7.1	32±11.5	5±3.5
PolarNet (Chen et al., 2023)	38.5 _{+1.7}	0+0.0	0+0.0	78+5.7	26 _{±8,2}	74+6.5	33±6.7	23 _{±8.4}
3D Diffuser Actor (Ke et al., 2024)	37.0+2.2	0+0.0	$0_{\pm 0.0}$	97 _{+2.7}	23+6.7	88+7.6	86+7.4	67 _{±9.8}
RVT2 (Goyal et al., 2024)	36.0+2.2	1+2.2	2+2.7	72+6.7	$42_{\pm 14.0}$	71+8.9	79+6.5	$5_{\pm 6.1}$
3D-LOTUS (Garcia et al., 2025)	$38.1_{\pm 1.1}$	$0_{\pm 0.0}$	$58_{\pm 8.1}$	$36_{\pm 9.7}$	$54_{\pm 10.7}$	85 _{±7.1}	42 _{±6.8}	$11_{\pm 6.6}$
3D-LOTUS++ (Garcia et al., 2025)	$41.5_{\pm 1.8}$	$1_{\pm 2.0}$	$29_{\pm 8.6}$	$93_{\pm 2.5}$	$50_{\pm 9.5}$	$99_{\pm 2.0}$	$52_{\pm 10.3}$	$16_{\pm 8.0}$
BridgeVLA (Li et al., 2025b)	43.8 $_{\pm 1.2}$	$0_{\pm 0.0}$	$1_{\pm 2.0}$	$95_{\pm 5.5}$	$77_{\pm 4.0}$	$54_{\pm 10.2}$	$68_{\pm 10.8}$	$74_{\pm 4.9}$
CLAP	49.6 $_{\pm 2.1}$	$3_{\pm 2.7}$	$9_{\pm 5.5}$	$92_{\pm 4.5}$	$35_{\pm 9.4}$	$79_{\pm 5.5}$	$56_{\pm 6.5}$	$1_{\pm 2.2}$
Method	Open Drawer2+0	Open Drawer3+0	OpenDrawer Long+0	OpenDrawer Long+1	OpenDrawer Long+2	OpenDrawer Long+3	Toilet SeatUp+0	Open Fridge+0
HiveFormer (Guhur et al., 2023)	$59_{\pm 11.9}$	$39_{\pm 11.9}$	78+8.4	82+4.5	49+4.2	57+11.5	6+4.2	$0_{\pm 0.0}$
PolarNet (Chen et al., 2023)	$91_{\pm 4.2}$	$29_{\pm 8.2}$	$84_{\pm 11.9}$	88 _{±5.7}	$63_{\pm 8.4}$	$37_{\pm 7.6}$	$2_{\pm 2.7}$	$4_{\pm 2.2}$
3D Diffuser Actor (Ke et al., 2024)	$19_{\pm 8.2}$	$1_{\pm 2.2}$	$15_{\pm 5.0}$	$35_{\pm 13.7}$	$26_{\pm 9.6}$	$79_{\pm 12.9}$	$0_{\pm 0.0}$	$7_{\pm 5.7}$
RVT2 (Goyal et al., 2024)	$81_{\pm 11.9}$	$0_{\pm 0.0}$	$84_{\pm 8.2}$	$39_{\pm 10.8}$	$11_{\pm 8.9}$	$75_{\pm 6.1}$	$7_{\pm 5.7}$	$0_{\pm 0.0}$
3D-LOTUS (Garcia et al., 2025)	$90_{\pm 3.2}$	$22_{\pm 8.1}$	$56_{\pm 13.9}$	$33_{\pm 11.2}$	$17_{\pm 8.1}$	$75_{\pm 6.3}$	$0_{\pm 0.0}$	$4_{\pm 5.8}$
3D-LOTUS++ (Garcia et al., 2025)	$70_{\pm 5.5}$	$41_{\pm 4.9}$	$72_{\pm 4.0}$	$52_{\pm 10.8}$	$23_{\pm 8.1}$	$78_{\pm 5.1}$	$8_{\pm 5.1}$	$0_{\pm 0.0}$
BridgeVLA (Li et al., 2025b)	$65_{\pm 6.3}$	$87_{\pm 6.0}$	$59_{\pm 8.6}$	$34_{\pm 8.0}$	$18_{\pm 10.3}$	$85_{\pm 8.4}$	$6_{\pm 5.8}$	$7_{\pm 2.5}$
CLAP	$68_{\pm 8.4}$	$87_{\pm 7.6}$	$44_{\pm 10.8}$	$94_{\pm 5.5}$	$14_{\pm 5.5}$	$76_{\pm 13.4}$	$7_{\pm 4.5}$	$3_{\pm 4.5}$
Method	OpenLaptop	Open	PutMoney	Open	Close	Close		
Method	Lid+0	Microwave+0	InSafe+2	Drawer+1	Drawer+0	Grill+0		
HiveFormer (Guhur et al., 2023)	$100_{\pm 0.0}$	$0_{\pm 0.0}$	$0_{\pm 0.0}$	$0_{\pm 0.0}$	$83_{\pm 5.7}$	$44_{\pm 10.8}$		
PolarNet (Chen et al., 2023)	$100_{\pm 0.0}$	$0_{\pm 0.0}$	$1_{\pm 2.2}$	$4_{\pm 4.2}$	$29_{\pm 11.9}$	$42_{\pm 11.5}$		
3D Diffuser Actor (Ke et al., 2024)	$100_{\pm 0.0}$	$0_{\pm 0.0}$	$2_{\pm 4.5}$	$0_{\pm 0.0}$	$66_{\pm 7.4}$	$65_{\pm 13.7}$		
RVT2 (Goyal et al., 2024)	$93_{\pm 5.7}$	$0_{\pm 0.0}$	$0_{\pm 0.0}$	$6_{\pm 2.2}$	$78_{\pm 8.4}$	$9_{\pm 4.2}$		
3D-LOTUS (Garcia et al., 2025)	$100_{\pm 0.0}$	$0_{\pm 0.0}$	$0_{\pm 0.0}$	$0_{\pm 0.0}$	$87_{\pm 8.1}$	$29_{\pm 6.6}$		
3D-LOTUS++ (Garcia et al., 2025)	$86_{\pm 6.6}$	$0_{\pm 0.0}$	$13_{\pm 8.1}$	$0_{\pm 0.0}$	$69_{\pm 5.8}$	$19_{\pm 13.9}$		
BridgeVLA (Li et al., 2025b)	$95_{\pm0.0}$	$0_{\pm 0.0}$	$2_{\pm 2.5}$	$0_{\pm 0.0}$	$58_{\pm 12.9}$	$35_{\pm 12.3}$		
CLAP	$78_{\pm 9.1}$	$0_{\pm 0.0}$	$76_{\pm 5.5}$	$96_{\pm 6.5}$	$84_{\pm 8.2}$	$40_{\pm 7.1}$		

Table 8: Per-task Success Rate on GemBench Level 3.

Place block in cup Original Postractors Distractors Dis

Figure 4: **Overview of the evaluation tasks in real-world experiments.** We evaluate the all these eight tasks across different variations and record the success rate.

Method	Avg.	Push Buttons4+1	Push Buttons4+2	Push Buttons4+3	TakeShoes OutOfBox+0	PutItems InDrawer+0	PutItems InDrawer+2
HiveFormer (Guhur et al., 2023)	$0_{\pm 0.0}$	$0_{\pm 0.0}$	$0_{\pm 0.0}$	$0_{\pm 0.0}$	$0_{\pm 0.0}$	0+0.0	$0_{\pm 0.0}$
PolarNet (Chen et al., 2023)	$0.1_{\pm 0.2}$	1±2.2	$0_{\pm 0.0}$	$0_{\pm 0.0}$	$0_{\pm 0.0}$	$0_{\pm 0.0}$	$0_{\pm 0.0}$
3D Diffuser Actor (Ke et al., 2024)	$0_{\pm 0.0}$	$0_{\pm 0.0}$	$0_{\pm 0.0}$	$0_{\pm 0.0}$	$0_{\pm 0.0}$	$0_{\pm 0.0}$	$0_{\pm 0.0}$
RVT2 (Goyal et al., 2024)	$0_{\pm 0.0}$	$0_{\pm 0.0}$	$0_{\pm 0.0}$	$0_{\pm 0.0}$	$0_{\pm 0.0}$	$0_{\pm 0.0}$	$0_{\pm 0.0}$
3D-LOTUS (Garcia et al., 2025)	$0.3_{\pm 0.3}$	$3_{\pm 4.0}$	$0_{\pm 0.0}$	$0_{\pm 0.0}$	$0_{\pm 0.0}$	$0_{\pm 0.0}$	$0_{\pm 0.0}$
3D-LOTUS++ (Garcia et al., 2025)	$17.4_{\pm0.4}$	$76_{\pm 7.4}$	$49_{\pm 8.6}$	$37_{\pm 8.1}$	$0_{\pm 0.0}$	$0_{\pm 0.0}$	$0_{\pm 0.0}$
BridgeVLA (Li et al., 2025b)	$0_{\pm 0.0}$	$0_{\pm 0.0}$	$0_{\pm 0.0}$	$0_{\pm 0.0}$	$0_{\pm 0.0}$	$0_{\pm 0.0}$	$0_{\pm 0.0}$
CLAP	$31.4_{\pm 0.6}$	$98_{\pm 2.7}$	$87_{\pm 4.5}$	$92_{\pm 5.7}$	$0_{\pm 0.0}$	$0_{\pm 0.0}$	$0_{\pm0.0}$
Method	PutItems	Tower4+1	Tower4+3	Stack	Stack	PutAllGroceries	
Wethod	InDrawer+4	10WC14+1	10wer4+3	Cups+0	Cups+3	InCupboard+0	
HiveFormer (Guhur et al., 2023)	$0_{\pm0.0}$	$0_{\pm 0.0}$	$0_{\pm 0.0}$	$0_{\pm 0.0}$	$0_{\pm0.0}$	$0_{\pm 0.0}$	
PolarNet (Chen et al., 2023)	$0_{\pm 0.0}$	$0_{\pm 0.0}$	$0_{\pm 0.0}$	$0_{\pm 0.0}$	$0_{\pm0.0}$	$0_{\pm 0.0}$	
3D Diffuser Actor (Ke et al., 2024)	$0_{\pm 0.0}$	$0_{\pm 0.0}$	$0_{\pm 0.0}$	$0_{\pm0.0}$	$0_{\pm0.0}$	$0_{\pm 0.0}$	
RVT2 (Goyal et al., 2024)	$0_{\pm 0.0}$	$0_{\pm 0.0}$	$0_{\pm 0.0}$	$0_{\pm0.0}$	$0_{\pm0.0}$	$0_{\pm 0.0}$	
3D-LOTUS (Garcia et al., 2025)	$0_{\pm 0.0}$	$0_{\pm 0.0}$	$0_{\pm 0.0}$	$0_{\pm0.0}$	$0_{\pm0.0}$	$0_{\pm 0.0}$	
3D-LOTUS++ (Garcia et al., 2025)	$0_{\pm 0.0}$	$17_{\pm 10.8}$	$30_{\pm 13.4}$	$0_{\pm 0.0}$	$0_{\pm0.0}$	$0_{\pm 0.0}$	
BridgeVLA (Li et al., 2025b)	$0_{\pm 0.0}$	$0_{\pm 0.0}$	$0_{\pm 0.0}$	$0_{\pm 0.0}$	$0_{\pm 0.0}$	$0_{\pm 0.0}$	
CLAP	$0_{\pm 0.0}$	$30_{\pm 7.1}$	$70_{\pm 6.1}$	$0_{\pm0.0}$	$0_{\pm 0.0}$	$0_{\pm 0.0}$	

Table 9: Per-task Success Rate on GemBench Level 4.